GEOLOGY | THE GEOLOGICAL SOCIETY OF AMERICA®

https://doi.org/10.1130/G54555.1

Manuscript received 20 February 2026
Revised manuscript received 17 June 2026
Manuscript accepted 10 July 2026

Published online 24 July 2026

Magnesium isotopes reveal hydroclimatically amplified low-latitude weathering during the early Toarcian

Zhong Han[1,2,*], Zhongya Hu[3], Jiaqi Guo[4], Mariano Parente[5], David B. Kemp[6], Mariano N. Remírez[7], Shuai Yuan[4], Xiang Li[4], Yongyun Hu[4], Hugh C. Jenkyns[8], Xinyang Chen[2], Marco Franceschi[9], and Xiumian Hu[10,*]

[1]Nanjing Institute of Geology and Palaeontology, Chinese Academy of Sciences, Nanjing 210008, China
[2]Institute of Sedimentary Geology, Chengdu University of Technology, Chengdu 610059, China
[3]School of Ocean and Earth Science, Tongji University, Shanghai 200092, China
[4]Department of Atmospheric and Oceanic Sciences, Peking University, Beijing 100871, China
[5]Department of Earth Sciences, Environment and Resources, University of Naples Federico II, 80126 Naples, Italy
[6]State Key Laboratory of Geomicrobiology and Environmental Changes, and Hubei Key Laboratory of Critical Zone Evolution, School of Earth and Planetary Sciences, China University of Geosciences, Wuhan 430074, China
[7]Department of Geosciences and Natural Resource Management, University of Copenhagen, 1350 Copenhagen, Denmark
[8]Department of Earth Sciences, University of Oxford, Oxford OX1 3AN, UK
[9]Department of Mathematics, Informatics and Geosciences, Università degli Studi di Trieste, 34128 Trieste, Italy
[10]School of Earth Sciences and Engineering, Nanjing University, Nanjing 210023, China

ABSTRACT

The Toarcian Stage of the Early Jurassic experienced extreme global warming, marine anoxia, hydrological intensification, and enhanced continental weathering driven by carbon emissions. Low-latitude silicate weathering, a key climate regulator, is highly sensitive to climatic shifts, yet its response to Toarcian warming remains poorly understood. We present magnesium isotopes (δ^{26}Mg) from carbonate-hosted silicates (acid-insoluble residues) in two geographically distinct, low-latitude carbonate platforms. Positive δ^{26}Mg excursions, indicative of intensified continental weathering, are observed immediately following the Pliensbachian–Toarcian (Pl–To) boundary, temporally coincident with Karoo large igneous province (LIP) emplacement. δ^{26}Mg values reached maxima during the onset interval of the Toarcian Oceanic Anoxic Event (T-OAE) negative carbon-isotope excursion (NCIE), temporally coincident with Ferrar LIP activity. The δ^{26}Mg pattern suggests that carbon emissions around the Pl–To boundary time did not immediately induce maximum weathering. Rather, cumulative carbon emissions were required to surpass a critical tipping point just above the Pl–To NCIE, triggering a weathering intensification that culminated during the T-OAE NCIE onset interval. Our data, coupled with climate simulations using the Community Earth System Model, indicate that in tectonically inactive regions, elevated temperatures and extreme runoff caused severe soil stripping, exposing the underlying bedrock to intense chemical weathering.

INTRODUCTION

The Toarcian Oceanic Anoxic Event (T-OAE; 183 Ma) represents one of the most extreme Phanerozoic hyperthermals. It is marked by a sustained positive carbon-isotope excursion interrupted by a prominent negative carbon-isotope excursion (NCIE) in the early Toarcian, closely following an earlier, smaller-scale NCIE at the Pliensbachian–Toarcian (Pl–To) boundary (Jenkyns, 2010; Littler et al., 2010). These carbon-cycle perturbations are ascribed to large-scale carbon emissions associated with the Karoo (southern Africa) and Ferrar (Antarctica) large igneous provinces (LIPs; Fig. 1A; Kemp et al., 2024a). This release triggered rapid global warming (Ruebsam et al., 2019), global expansion of marine anoxia (Dickson et al., 2017; Them et al., 2018; Han et al., 2023; Remírez et al., 2024), intensified hydrological cycling, and enhanced continental weathering (Cohen et al., 2004; Han et al., 2018; Kemp et al., 2020, 2024b).

Silicate weathering is a critical negative feedback mechanism regulating the global carbon cycle and climate over geological time scales. During the T-OAE, rapid shifts in ^{87}Sr/^{86}Sr, ^{187}Os/^{188}Os$_i$, and $\delta^{44/40}$Ca indicate a marked increase in global continental weathering rates (McArthur et al., 2000; Brazier et al., 2015; Them et al., 2017; Kemp et al., 2020). Although these proxies reflect global seawater changes, and thus globally averaged weathering rates, recent work has suggested spatial heterogeneity in silicate weathering over relatively short time scales, with significant low-latitude contributions (Deng et al., 2022). However, the intensity and evolution of low-latitude chemical weathering during the T-OAE remain poorly constrained. Magnesium isotopes (δ^{26}Mg) have emerged as reliable tracers for local or regional chemical weathering intensity (i.e., the degree of chemical alteration of the regolith), because silicate weathering preferentially releases light Mg isotopes into fluids, leaving weathered residues enriched in heavy isotopes (Teng et al., 2010; Liu et al., 2014). We utilize δ^{26}Mg in acid-insoluble residues in both the Northern and Southern Hemispheres, coupled with climate simulations, to elucidate the variations and drivers of low-latitude silicate weathering across the T-OAE.

Zhong Han https://orcid.org/0000-0002-8690-454X
*zhonghan@nigpas.ac.cn; huxm@nju.edu.cn

CITATION: Han, Z., et al., 2026, Magnesium isotopes reveal hydroclimatically amplified low-latitude weathering during the early Toarcian: Geology, v. XX, p. , https://doi.org/10.1130/G54555.1

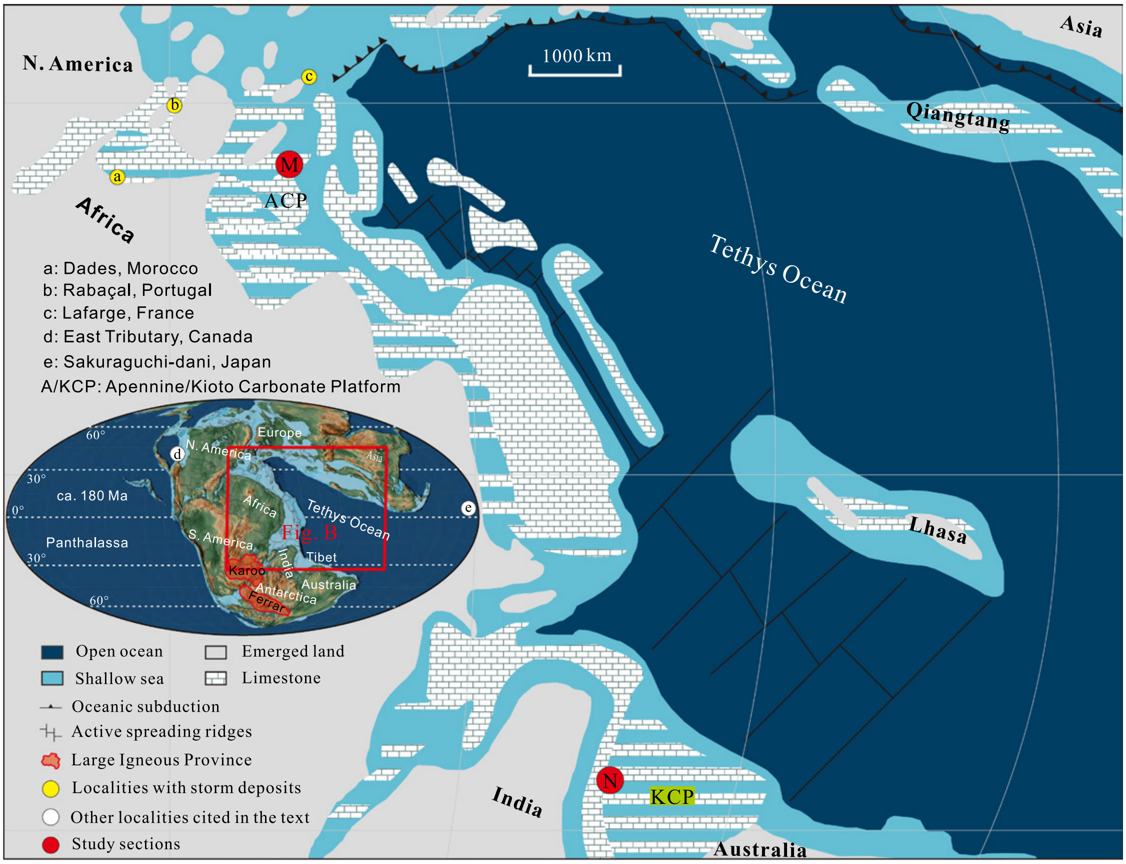

Figure 1. Toarcian paleogeography showing the Nianduo (N; Tibet) and Mercato San Severino (M; Italy) sections (this study) and other key locations (modified from Han et al. [2018] and Scotese [2021]).

MATERIALS AND METHODS

We examined the uppermost Pliensbachian to lower Toarcian of the Nianduo section from the Tibetan Kioto Carbonate Platform at a paleolatitude of ~22–26°S, and coeval strata of the Mercato San Severino (MSS) section from the Italian Apennine Carbonate Platform at ~20°N (Fig. 1B). These carbonate platforms formed in clear, warm, low-latitude waters, and trapped fine-grained terrigenous silicates delivered via fluvial or eolian transport from weathered watersheds.

The Pl–To boundary age and stratigraphically higher T-OAE NCIE in both platforms are well-constrained (Trecalli et al., 2012; Han et al., 2018, 2023). We analyzed δ^{26}Mg and elemental compositions of carbonate-hosted silicates (acid-insoluble residues) extracted from 49 samples (Nianduo: n = 29; MSS: n = 20). As confirmed by geochemical and X-ray diffraction (XRD) data, these residues represent a continentally derived detrital mixture of transported secondary weathering products and residual primary minerals. Mineralogical compositions were determined on a subset of these samples (Nianduo: n = 18; MSS: n = 15). Additionally, we used the Community Earth System Model (CESM; https://www.cesm.ucar.edu) to evaluate early Toarcian global mean climate patterns. Detailed age constraints, residue validation, and all analytical and modeling methodologies are provided in the Supplemental Material[1].

RESULTS

The Nianduo section exhibits relatively stable δ^{26}Mg values (−1.54‰ to −1.14‰) in the uppermost Pliensbachian (−28.6 m to −4.6 m), followed by a rapid rise from −1.26‰ to −0.16‰ (−4.6 m to 4.8 m; Fig. 2). This Mg-isotope excursion (MIE) clearly post-dates the Pl–To NCIE (−10 m to −5 m) but starts below the T-OAE NCIE onset level (−2 m). It peaks within the T-OAE NCIE onset interval (−2 m to −3 m), gradually declines from −0.39‰ to −0.86‰ (5.6–31.4 m), and then continues to drift downward with small oscillations between −0.49‰ and −0.95‰ following the NCIE. By contrast, the MSS section records overall higher δ^{26}Mg (−0.13‰ to +0.30‰). The uppermost Pliensbachian exhibits relatively constant values (0.09‰–0.26‰), with a minor positive excursion at the Pl–To boundary (112 m). Higher up, δ^{26}Mg increases from 0.11‰ to 0.30‰ immediately below the T-OAE NCIE onset level, followed by an overall declining trend reaching −0.13‰.

[1]Supplemental Material. Detailed analytical methods, evaluations of primary geochemical signals, extended discussions on stratigraphy and hydroclimate, and supplementary figures. Please visit https://doi.org/10.1130/GEOL.S.33006950 to access the supplemental material; contact editing@geosociety.org with any questions.

DISCUSSION AND CONCLUSIONS

Enhanced Low-Latitude Chemical Weathering During the Early Toarcian

The δ^{26}Mg variations are unrelated to diagenesis, lithological and/or provenance changes, or volcanic inputs, as evidenced by stable conservative trace-element ratios (e.g., Th/Sc, Zr/Sc), uniform rare earth element (REE) patterns, consistent detrital mineral assemblages, and a lack of correlation between δ^{26}Mg and carbonate content (Figs. S1–S3 in the Supplemental Material). Furthermore, while the lower δ^{26}Mg baseline of Nianduo compared to MSS primarily reflects chlorite-dominated Mg minerals with isotopically light compositions, statistical and mass-balance analyses confirm that the positive δ^{26}Mg excursions are not artifacts of chlorite fluctuations (Figs. S1 and S3) but represent genuine shifts in weathering. Such signatures depend on weathering intensity and protolith composition, resulting in heterogeneous fractionation, which influences both the baselines and MIE magnitudes (Teng et al., 2010; Liu et al., 2014). Consequently, relative changes in δ^{26}Mg, rather than absolute values, serve as tracers for regional changes in weathering intensity. Global weathering profiles confirm that intensified weathering elevates δ^{26}Mg

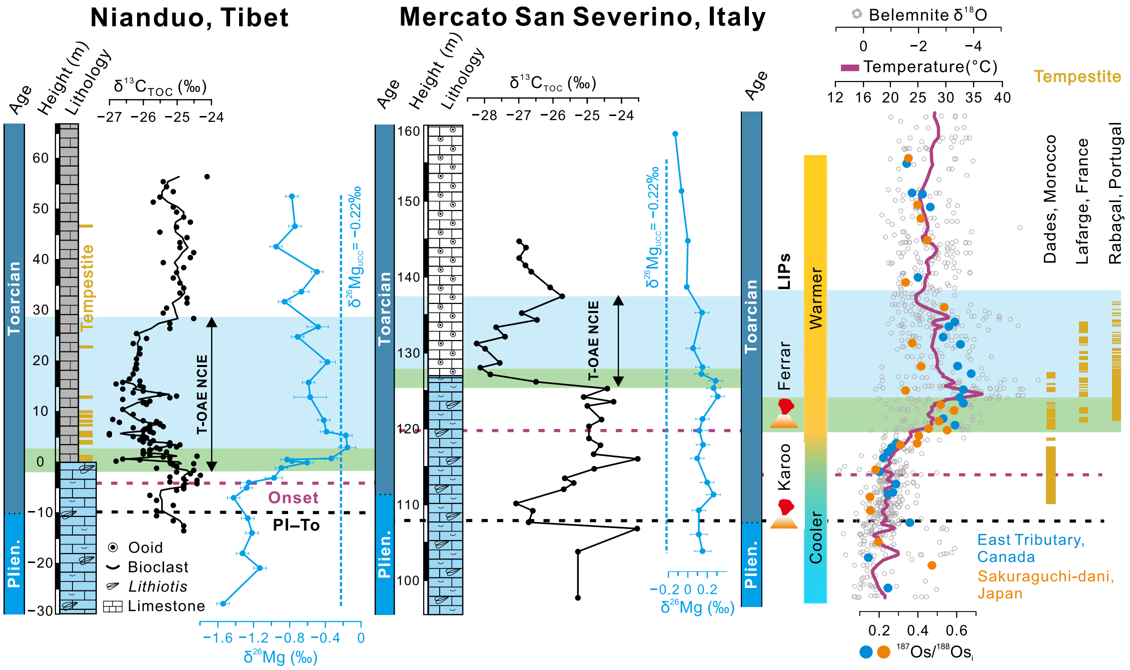

Figure 2. Stratigraphic correlation of proxies across the studied Pliensbachian–Toarcian (Pl–To) interval. The Nianduo and Mercato San Severino sections show δ^{26}Mg data (indicative of intensified continental weathering). $\delta^{26}Mg_{UCC}$—Mg isotopic composition of the upper continental crust. Lithostratigraphy, $\delta^{13}C_{TOC}$ (TOC—total organic carbon), and storm records are from Han et al. (2018) and Trecalli et al. (2012), respectively. Dashed lines mark the Pl–To boundary (black) and onset of δ^{26}Mg rise (purple). Colored bands indicate Toarcian Oceanic Anoxic Event (T-OAE) negative carbon-isotope excursion (NCIE) onset (green) and main interval (blue). Global references include Os isotopes (Them et al., 2017; Kemp et al., 2020), locally weighted scatterplot smoothing (LOWESS)–smoothed belemnite δ^{18}O and temperature (Ruebsam et al., 2019), and the age model, large igneous province (LIP) ages, climate states, and compiled tempestites (Kemp et al., 2024a, 2024b).

in secondary products (Teng et al., 2010; Ryu et al., 2021), a pattern corroborated by detrital records generated during the Marinoan glaciation (Huang et al., 2016) and Early Triassic warming (Chen et al., 2020a). Mechanistically, this process reflects the preferential incorporation of heavy δ^{26}Mg into secondary phyllosilicates due to crystallographic discrimination during Mg-O bond reorganization between primary and secondary minerals (Hindshaw et al., 2020; Ryu et al., 2021). Therefore, the δ^{26}Mg increase, coupled with an overall Mg/Ti decrease (indicative of Mg depletion) in both sections (Fig. S1), indicates enhanced chemical weathering. Using the T-OAE NCIE as a chronostratigraphic marker, the rising δ^{26}Mg trend in MSS terminates earlier (at the NCIE onset) than in Nianduo. These localized discrepancies could be attributed to stratigraphic incompleteness, typical of shallow-water platform carbonates (see the Supplemental Material). An unconformity at MSS removed strata recording the continued δ^{26}Mg rise, truncating the MIE peak values, while a condensed interval at Nianduo likely obscures the Pl–To boundary precursor anomaly. Overall, these findings imply a synchronous intensification of low-latitude chemical weathering in both hemispheres, initiating immediately following the Pl–To boundary, peaking during the onset interval of the T-OAE NCIE, and declining during the NCIE recovery. This pattern aligns with the Os-isotope record from Japan (Kemp et al., 2020), although other records exhibit a more pronounced period of elevated values later within the T-OAE NCIE interval (Fig. 2).

New high-precision U-Pb geochronologies link the Karoo LIP with the Pl–To NCIE, and the Ferrar LIP with the T-OAE NCIE (Al-Suwaidi et al., 2022; Kemp et al., 2024a). Critically, the MIE initiates immediately after the Pl–To NCIE but slightly before the T-OAE NCIE (Fig. 2). This delayed response implies that initial Pl–To carbon emissions did not immediately trigger system-wide disruption. Instead, cumulative atmospheric carbon was required to surpass a critical threshold just above the Pl–To NCIE interval, thereby triggering the abrupt and severe environmental and biological crises that culminated during the T-OAE NCIE onset interval. The rapidity of the environmental shifts at the T-OAE onset, as consistently observed across sedimentological, biological, and geochemical proxies, points to a nonlinear system response to the cumulative forcing of the Karoo and Ferrar LIPs.

Hydroclimate-Driven Enhanced Continental Weathering

The positive MIE proximal to the end of the Pl–To NCIE to within the onset of the T-OAE NCIE likely spanned >200 k.y. (Al-Suwaidi et al., 2022; Kemp et al., 2024a). The MIE culmination within the T-OAE NCIE onset (characterized by peak warmth, globally elevated weathering, and storm deposits) underlines hydroclimatic extremes as the primary driver of regional weathering intensity. In tectonically quiescent study regions (Trecalli et al., 2012; Han et al., 2018), thick soil mantles typically shield the underlying bedrock from further chemical alteration. Under the warm conditions of the early Toarcian, intensified runoff and storminess likely stripped this shielding soil cover, exposing the bedrock to intense weathering. Crucially, this severe soil-erosion mechanism is independently supported by the massive influx of terrestrially derived mercury into various marine basins during this interval (Them et al., 2019). Consequently, the physical supply of unweathered bedrock became directly coupled with hydroclimatic extremes.

To explore the above mechanism, we used the CESM to simulate Toarcian climate conditions parameterized by reconstructed CO_2 concentrations (see the Supplemental Material). Simulations show that increasing CO_2 from 1× (280 ppm, Pl–To boundary) to 2× (560 ppm, T-OAE NCIE onset) and 4× (1120 ppm, NCIE recovery) pre-industrial levels causes pronounced expansion of poleward warmth (Figs. S4A–S4C). Specifically, doubling CO_2 from 1× to 2× increases global mean temperature by 4.3 °C, and a further doubling to 4× causes an additional 6.3 °C rise (Figs. 3A and 3B). Low-latitude continental regions warmed 3–5 °C per step (6–10 °C cumulative), in line with proxy-based reconstructions (Ruebsam et al., 2019). Warming promotes continental weathering by accelerating chemical reactions (Arrhenius effect), and through mechanisms such as thermal stress fatigue and shock, and enhanced biotic activity (Chen et al., 2020b; Deng et al., 2022; Brantley et al., 2023). However, these impacts are negligible in the soil-mantled landscapes likely characteristic of our tectonically inactive study areas, where fresh minerals would have been inaccessible (Maher and Chamberlain,

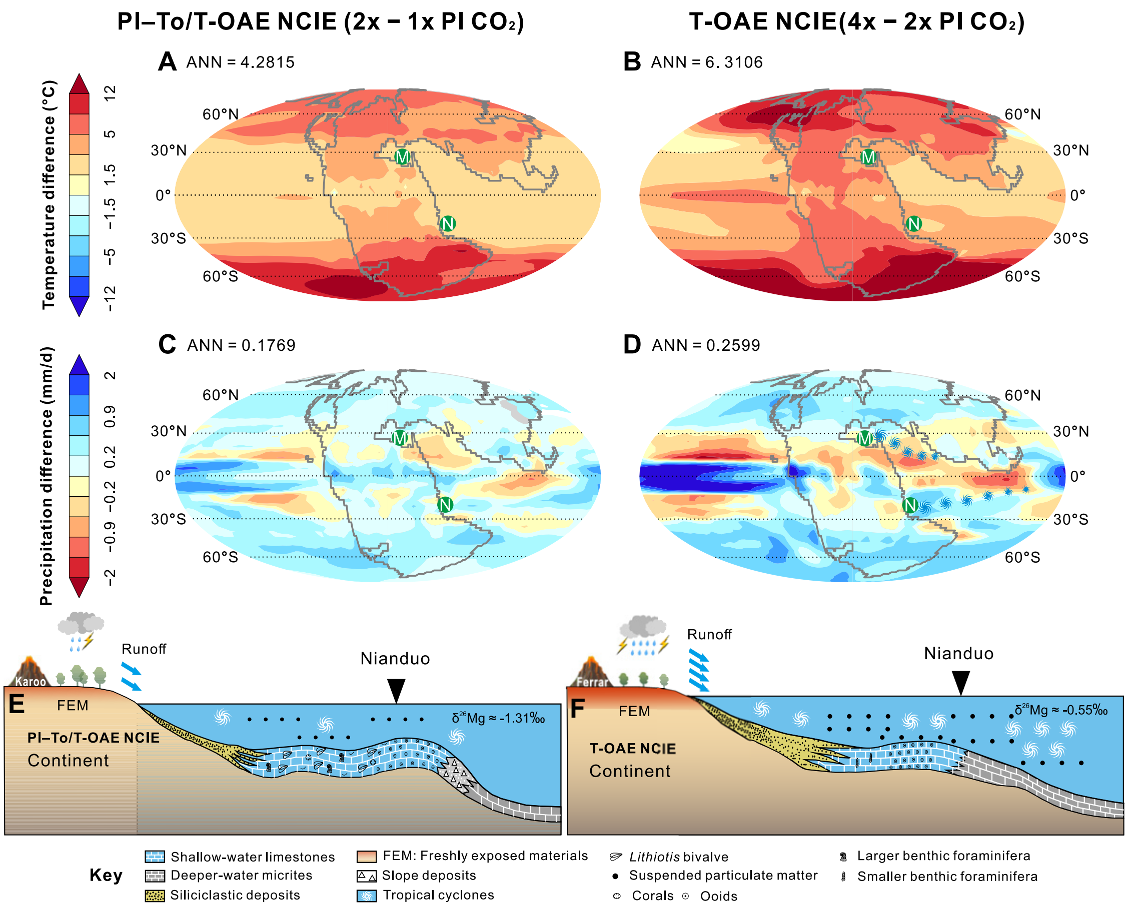

Figure 3. Climate simulations and weathering models for the Pliensbachian–Toarcian (Pl–To) Toarcian Oceanic Anoxic Event (T-OAE) negative carbon-isotope excursion (NCIE). (A–D) Simulated changes in annual (ANN) mean surface temperature (°C) and precipitation (mm) for 2× versus 1× pre-industrial (PI) CO_2, and 4× versus 2× PI CO_2 (~280 ppm). Tropical cyclone centers in panel D are from Yan et al. (2023). N—Nianduo section (Tibet); M—Mercato San Severino section (Italy). (E, F) Conceptual framework linking weathering, large igneous provinces (Karoo and Ferrar), storm activities, precipitation, runoff, and freshly exposed materials (FEM) on the Tibetan Kioto Carbonate Platform from the Pl–To boundary to the T-OAE NCIE interval.

2014; Brantley et al., 2023). Thus, rapid warming alone was likely insufficient to drive the observed weathering pulse without a mechanism to strip the shielding cover. Our simulations do, however, show that global annual mean precipitation expanded poleward and landward (Figs. S4D–S4F), increasing by 0.18 mm/d (1× to 2× pre-industrial CO_2) and 0.26 mm/d (2× to 4× CO_2) (Figs. 3C and 3D). In detail, the simulations reveal a spatially divergent response at low latitudes. Specifically, mean annual precipitation in the Nianduo area exhibited only a small increase, while the MSS area experienced slight drying, reinforcing the archetypal "dry gets drier, wet gets wetter" paradigm. Our simulations represent mean climatology and do not explicitly resolve individual extreme weather events like tropical cyclones. To bridge this gap, we rely on recent high-resolution modeling (Yan et al., 2023), which demonstrates that Toarcian warming intensified tropical cyclones and hydroclimate volatility, even in regions experiencing mean annual drying. This theoretical increase in extreme storminess is corroborated by independent sedimentological evidence, particularly the increased abundance of tempestites in both study areas (Figs. 1 and 2; Krencker et al., 2015; Han et al., 2018). This hydroclimate volatility thus explains our evidence of enhanced weathering in these seemingly arid to semi-arid settings. The existence of a sparse, vulnerable soil and vegetation cover in the hinterland is supported by episodic pulses of terrestrial input and associated organic matter mixing into otherwise pure carbonates of the Kioto Carbonate Platform (Han et al., 2018). Episodic and extreme tropical cyclones and flash floods would have stripped this sparse soil cover, exposing fresh bedrock to intense chemical attack under elevated temperatures.

The integrated $\delta^{26}Mg$ data, climate modeling, and storm records demonstrate a causal linkage between hydrological intensification and weathering. Enhanced precipitation, particularly from tropical cyclones, would have generated substantial runoff. Concurrently, warming following the Clausius–Clapeyron equation (~7% atmospheric moisture rise per 1 °C) potentially amplified global moisture content by ~40% during the T-OAE (conservative ~5 °C warming; Fig. 2), further intensifying rainfall frequency and magnitude (Swain et al., 2025). The intensified hydrological cycling at low latitudes would have fostered extreme flooding, landslides, and enhanced physical denudation, thereby increasing globally integrated chemical weathering fluxes (Ferrier et al., 2013; Grande et al., 2021). Although rapid erosion typically reduces chemical weathering intensity by limiting regolith residence time (West et al., 2005), the positive $\delta^{26}Mg$ excursion confirms that local weathering intensity significantly increased and then remained high. We attribute this effect to extreme hydroclimatic forcing: elevated temperatures and enhanced runoff accelerated reaction kinetics sufficiently to produce highly weathered residues despite short residence times. Notably, our CESM simulations indicate that this hydroclimate-driven weathering amplification was likely restricted to low latitudes. While mid- to high latitudes also experienced increased rainfall (Fig. 3), temperatures remained moderate (<14 °C even at 4× pre-industrial CO_2). Lacking the thermal driver (Arrhenius effect) to accelerate chemical kinetics, physical denudation in these regions likely outpaced chemical alteration, resulting in the export of immature, weakly weathered sediments. By contrast, low-latitude regions, characterized by elevated temperatures and significantly intensified hydrological cycling, played a pivotal role in regulating the carbon cycle during this extreme greenhouse period.

ACKNOWLEDGEMENTS

This work is funded by the Chinese National Key R&D Program (grant 2023YFF0804000), the National Natural Science Foundation of China (grants 42272116 and 41888201), the Chinese Research Fund for International Scientists (grant W2531028), and the Italian Ministry of University and Research (grant 4362017RX9XXXY). This manuscript is a contribution to International Geoscience Programme (IGCP) 739. We thank editor Mark Patzkowsky, reviewers Thomas Algeo, Guillaume Suan, and Alex Dickson, and three anonymous reviewers for their constructive comments that greatly improved this manuscript.

REFERENCES CITED

Al-Suwaidi, A.H., et al., 2022, New age constraints on the Lower Jurassic Pliensbachian–Toarcian Boundary at Chacay Melehue (Neuquén Basin, Argentina): Scientific Reports, v. 12, 4975, https://doi.org/10.1038/s41598-022-07886-x.

Brantley, S.L., Shaughnessy, A., Lebedeva, M.I., and Balashov, V.N., 2023, How temperature-dependent silicate weathering acts as Earth's geological thermostat: Science, v. 379, p. 382–389, https://doi.org/10.1126/science.add2922.

Brazier, J.M., Suan, G., Tacail, T., Simon, L., Martin, J.E., Mattioli, E., and Baiter, V., 2015, Calcium isotope evidence for dramatic increase of continental weathering during the Toarcian oceanic anoxic event (Early Jurassic): Earth and Planetary Science Letters, v. 411, p. 164–176, https://doi.org/10.1016/j.epsl.2014.11.028.

Chen, X., Teng, F., Huang, K., and Algeo, T.J., 2020a, Intensified chemical weathering during Early Triassic revealed by magnesium isotopes: Geochimica et Cosmochimica Acta, v. 287, p. 263–276, https://doi.org/10.1016/j.gca.2020.02.035.

Chen, Y., Hedding, D.W., Li, X., Greyling, A.C., and Li, G., 2020b, Weathering dynamics of Large Igneous Provinces (LIPs): A case study from the Lesotho Highlands: Earth and Planetary Science Letters, v. 530, https://doi.org/10.1016/j.epsl.2019.115871.

Cohen, A.S., Coe, A.L., Harding, S.M., and Schwark, L., 2004, Osmium isotope evidence for the regulation of atmospheric CO_2 by continental weathering: Geology, v. 32, p. 157–160, https://doi.org/10.1130/G20158.1.

Deng, K., Yang, S., and Guo, Y., 2022, A global temperature control of silicate weathering intensity: Nature Communications, v. 13, 1781, https://doi.org/10.1038/s41467-022-29415-0.

Dickson, A.J., Gill, B.C., Ruhl, M., Jenkyns, H.C., Porcelli, D., Idiz, E., Lyons, T.W., and van den Boorn, S.H.J.M., 2017, Molybdenum-isotope chemostratigraphy and paleoceanography of the Toarcian Oceanic Anoxic Event (Early Jurassic): Paleoceanography, v. 32, p. 813–829, https://doi.org/10.1002/2016PA003048.

Ferrier, K.L., Huppert, K.L., and Perron, J.T., 2013, Climatic control of bedrock river incision: Nature, v. 496, p. 206–209, https://doi.org/10.1038/nature11982.

Grande, A., Schmidt, A.H., Bierman, P.R., Corbett, L.B., López-Lloreda, C., Willenbring, J., McDowell, W.H., and Caffee, M.W., 2021, Landslides, hurricanes, and sediment sourcing impact basin-scale erosion estimates in Luquillo, Puerto Rico: Earth and Planetary Science Letters, v. 562, https://doi.org/10.1016/j.epsl.2021.116821.

Han, Z., Hu, X., Kemp, D.B., and Li, J., 2018, Carbonate-platform response to the Toarcian Oceanic Anoxic Event in the southern hemisphere: Implications for climatic change and biotic platform demise: Earth and Planetary Science Letters, v. 489, p. 59–71, https://doi.org/10.1016/j.epsl.2018.02.017.

Han, Z., Hu, X., Newton, R.J., He, T., Mills, B.J.W., Jenkyns, H.C., Ruhl, M., and Jamieson, R.A., 2023, Spatially heterogenous seawater $\delta^{34}S$ and global cessation of Ca-sulfate burial during the Toarcian oceanic anoxic event: Earth and Planetary Science Letters, v. 622, https://doi.org/10.1016/j.epsl.2023.118404.

Hindshaw, R.S., Tosca, R., Tosca, N.J., and Tipper, E.T., 2020, Experimental constraints on Mg isotope fractionation during clay formation: Implications for the global biogeochemical cycle of Mg: Earth and Planetary Science Letters, v. 531, https://doi.org/10.1016/j.epsl.2019.115980.

Huang, K.-J., Teng, F.-Z., Shen, B., Xiao, S., Lang, X., Ma, H.-R., Fu, Y., and Peng, Y., 2016, Episode of intense chemical weathering during the termination of the 635 Ma Marinoan glaciation: Proceedings of the National Academy of Sciences of the United States of America, v. 113, p. 14,904–14,909, https://doi.org/10.1073/pnas.1607712113.

Jenkyns, H.C., 2010, Geochemistry of oceanic anoxic events: Geochemistry, Geophysics, Geosystems, v. 11, Q03004, https://doi.org/10.1029/2009GC002788.

Kemp, D.B., Selby, D., and Izumi, K., 2020, Direct coupling between carbon release and weathering during the Toarcian oceanic anoxic event: Geology, v. 48, p. 976–980, https://doi.org/10.1130/G47509.1.

Kemp, D.B., Ramezani, J., Izumi, K., Al-Suwaidi, A., Huang, C., Chen, W., and Zhu, Y., 2024a, The timing and duration of large-scale carbon release in the Early Jurassic: Geology, v. 52, p. 891–895, https://doi.org/10.1130/G52457.1.

Kemp, D.B., et al., 2024b, Global hydroclimate perturbations during the Toarcian oceanic anoxic event: Earth-Science Reviews, v. 258, https://doi.org/10.1016/j.earscirev.2024.104946.

Krencker, F.N., Bodin, S., Suan, G., Heimhofer, U., Kabiri, L., and Immenhauser, A., 2015, Toarcian extreme warmth led to tropical cyclone intensification: Earth and Planetary Science Letters, v. 425, p. 120–130, https://doi.org/10.1016/j.epsl.2015.06.003.

Littler, K., Hesselbo, S.P., and Jenkyns, H.C., 2010, A carbon-isotope perturbation at the Pliensbachian–Toarcian boundary: Evidence from the Lias Group, NE England: Geological Magazine, v. 147, p. 181–192, https://doi.org/10.1017/S0016756809990458.

Liu, X.-M., Teng, F.-Z., Rudnick, R.L., McDonough, W.F., and Cummings, M.L., 2014, Massive magnesium depletion and isotope fractionation in weathered basalts: Geochimica et Cosmochimica Acta, v. 135, p. 336–349, https://doi.org/10.1016/j.gca.2014.03.028.

Maher, K., and Chamberlain, C.P., 2014, Hydrologic regulation of chemical weathering and the geologic carbon cycle: Science, v. 343, p. 1502–1504, https://doi.org/10.1126/science.1250770.

McArthur, J., Donovan, D., Thirlwall, M., Fouke, B., and Mattey, D., 2000, Strontium isotope profile of the early Toarcian (Jurassic) oceanic anoxic event, the duration of ammonite biozones, and belemnite palaeotemperatures: Earth and Planetary Science Letters, v. 179, p. 269–285, https://doi.org/10.1016/S0012-821X(00)00111-4.

Remírez, M.N., Gilleaudeau, G.J., Gan, T., Kipp, M.A., Tissot, F.L.H., Kaufman, A.J., and Parente, M., 2024, Carbonate uranium isotopes record global expansion of marine anoxia during the Toarcian Oceanic Anoxic Event: Proceedings of the National Academy of Sciences of the United States of America, v. 121, https://doi.org/10.1073/pnas.2406032121.

Ruebsam, W., Mayer, B., and Schwark, L., 2019, Cryosphere carbon dynamics control early Toarcian global warming and sea level evolution: Global and Planetary Change, v. 172, p. 440–453, https://doi.org/10.1016/j.gloplacha.2018.11.003.

Ryu, J.-S., Vigier, N., Derry, L., and Chadwick, O.A., 2021, Variations of Mg isotope geochemistry in soils over a Hawaiian 4 Myr chronosequence: Geochimica et Cosmochimica Acta, v. 292, p. 94–114, https://doi.org/10.1016/j.gca.2020.09.024.

Scotese, C., 2021, An atlas of Phanerozoic paleogeographic maps: The seas come in and the seas go out: Annual Review of Earth and Planetary Sciences, v. 49, p. 679–728, https://doi.org/10.1146/annurev-earth-081320-064052.

Swain, D.L., Prein, A.F., Abatzoglou, J.T., Albano, C.M., Brunner, M., Diffenbaugh, N.S., Singh, D., Skinner, C.B., and Touma, D., 2025, Hydroclimate volatility on a warming Earth: Nature Reviews: Earth & Environment, v. 6, p. 35–50, https://doi.org/10.1038/s43017-024-00624-z.

Teng, F.-Z., Li, W.-Y., Rudnick, R.L., and Gardner, L.R., 2010, Contrasting lithium and magnesium isotope fractionation during continental weathering: Earth and Planetary Science Letters, v. 300, p. 63–71, https://doi.org/10.1016/j.epsl.2010.09.036.

Them, T.R., Gill, B.C., Selby, D., Gröcke, D.R., Friedman, R.M., and Owens, J.D., 2017, Evidence for rapid weathering response to climatic warming during the Toarcian Oceanic Anoxic Event: Scientific Reports, v. 7, 5003, https://doi.org/10.1038/s41598-017-05307-y.

Them, T.R., Gill, B.C., Caruthers, A.H., Gerhardt, A.M., Gröcke, D.R., Lyons, T.W., Marroquín, S.M., Nielsen, S.G., Trabucho Alexandre, J.P., and Owens, J.D., 2018, Thallium isotopes reveal protracted anoxia during the Toarcian (Early Jurassic) associated with volcanism, carbon burial, and mass extinction: Proceedings of the National Academy of Sciences of the United States of America, v. 115, p. 6596–6601, https://doi.org/10.1073/pnas.1803478115.

Them, T.R., Jagoe, C.H., Caruthers, A.H., Gill, B.C., Grasby, S.E., Gröcke, D.R., Yin, R., and Owens, J.D., 2019, Terrestrial sources as the primary delivery mechanism of mercury to the oceans across the Toarcian Oceanic Anoxic Event (Early Jurassic): Earth and Planetary Science Letters, v. 507, p. 62–72, https://doi.org/10.1016/j.epsl.2018.11.029.

Trecalli, A., Spangenberg, J., Adatte, T., Föllmi, K.B., and Parente, M., 2012, Carbonate platform evidence of ocean acidification at the onset of the early Toarcian oceanic anoxic event: Earth and Planetary Science Letters, v. 357–358, p. 214–225, https://doi.org/10.1016/j.epsl.2012.09.043.

West, A.J., Galy, A., and Bickle, M., 2005, Tectonic and climatic controls on silicate weathering: Earth and Planetary Science Letters, v. 235, p. 211–228, https://doi.org/10.1016/j.epsl.2005.03.020.

Yan, Q., Li, X., Kemp, D.B., Guo, J., Zhang, Z., and Hu, Y., 2023, Elevated atmospheric CO_2 drove an increase in tropical cyclone intensity during the early Toarcian hyperthermal: Proceedings of the National Academy of Sciences of the United States of America, v. 120, https://doi.org/10.1073/pnas.2301018120.

Printed in the USA